Abdominal Radiology (2019) 44:2233–2243
https://doi.org/10.1007/s00261-019-01936-1

PELVIS

Revisiting quantitative multi-parametric MRI of benign prostatic hyperplasia and its differentiation from transition zone cancer

Aritrick Chatterjee[1] · Alexander J. Gallan[2] · Dianning He[1,3] · Xiaobing Fan[1] · Devkumar Mustafi[1] · Ambereen Yousuf[1] · Tatjana Antic[2] · Gregory S. Karczmar[1] · Aytekin Oto[1]

Published online: 6 April 2019
© Springer Science+Business Media, LLC, part of Springer Nature 2019

Abstract

Purpose This study investigates the multiparametric MRI (mpMRI) appearance of different types of benign prostatic hyperplasia (BPH) and whether quantitative mpMRI is effective in differentiating between prostate cancer (PCa) and BPH.

Materials and methods Patients ($n=60$) with confirmed PCa underwent preoperative 3T MRI. T2-weighted, multi-echo T2-weighted, diffusion weighted and dynamic contrast enhanced images (DCE) were obtained prior to undergoing prostatectomy. PCa and BPH (cystic, glandular or stromal) were identified in the transition zone and matched with MRI. Quantitative mpMRI metrics: T2, ADC and DCE-MRI parameters using an empirical mathematical model were measured.

Results ADC values were significantly lower ($p<0.001$) in PCa compared to all BPH types and can differentiate between PCa and BPH with high accuracy (AUC = 0.87, $p<0.001$). T2 values were significantly lower ($p<0.001$) in PCa compared to cystic BPH only, while glandular ($p=0.27$) and stromal BPH ($p=0.99$) showed no significant difference from PCa. BPH mimics PCa in the transition zone on DCE-MRI evidenced by no significant difference between them. mpMRI values of glandular (ADC = 1.31 ± 0.22 μm^2/ms, T2 = 115.7 ± 37.3 ms) and cystic BPH (ADC = 1.92 ± 0.43 μm^2/ms, T2 = 242.8 ± 117.9 ms) are significantly different. There was no significant difference in ADC ($p=0.72$) and T2 ($p=0.46$) between glandular and stromal BPH.

Conclusions Multiparametric MRI and specifically quantitative ADC values can be used for differentiating PCa and BPH, improving PCa diagnosis in the transition zone. However, DCE-MRI metrics are not effective in distinguishing PCa and BPH. Glandular BPH are not hyperintense on ADC and T2 as previously thought and have similar quantitative mpMRI measurements to stromal BPH. Glandular and cystic BPH appear differently on mpMRI and are histologically different.

Keywords Prostate cancer · Benign prostatic hyperplasia · Cystic · Stromal · Glandular

✉ Aytekin Oto
aoto@radiology.bsd.uchicago.edu

Aritrick Chatterjee
aritrick@uchicago.edu

Alexander J. Gallan
Alexander.Gallan@uchospitals.edu

Dianning He
dianninghe@uchicago.edu

Xiaobing Fan
xfan@uchicago.edu

Devkumar Mustafi
dmustafi@uchicago.edu

Ambereen Yousuf
ayousuf@radiology.bsd.uchicago.edu

Tatjana Antic
Tatjana.Antic@uchospitals.edu

Gregory S. Karczmar
gskarczm@uchicago.edu

[1] Department of Radiology, University of Chicago, 5841 South Maryland Avenue, Chicago, IL 60637, USA

[2] Department of Pathology, University of Chicago, 5841 South Maryland Avenue, Chicago, IL, USA

[3] Sino-Dutch Biomedical and Information Engineering School, Northeastern University, No. 3-11, Wenhua Road, Heping District, Shenyang, People's Republic of China

Introduction

Prostate cancer (PCa) is the most common non-cutaneous cancer in men in the USA with one out of nine men affected by it [1]. Multiparametric magnetic resonance imaging (mpMRI) is increasingly being used in the detection and local staging of PCa and for guiding biopsies. While the majority of PCa occur in the peripheral zone, up to 30% may reside in the transition zone [2–4]. The transition zone (TZ) is also the site of benign prostatic hyperplasia (BPH), a non-cancerous, often nodular increase in prostatic glands and stroma which can result in urinary obstruction. BPH is a common condition in older men with a prevalence of pathological BPH in over 50% of men by the age of 60 years, and over 90% in men over 80 years [5]. BPH have been shown to mimic PCa on mpMRI, therefore making PCa detection in the transition zone problematic [6–9]. Not only does this lead to unnecessary biopsies, but also numerous cancer lesions remain undetected which show progression [10, 11].

The transition zone is highly heterogeneous with different types of BPH, and yet, most MR studies take a representative measurement considering the transition zone to be homogenous [12, 13]. Few studies have noted BPH were either stromal or glandular. Glandular BPH has been shown to be hyperintense and stromal BPH to be hypointense on T2-weighted imaging [8, 14], while glandular BPH had significantly higher ADC values compared to stromal BPH [8]. These studies considered cystic BPH as a form of glandular BPH, despite one previous study having shown cystic BPH as a hyperintense regions on T2-weighted (T2 W) MRI with respect to other BPH types in an era when mpMRI of the prostate was not utilized [6]. More recently, Thai et al. [15] contributed novel information to the literature by reporting specific application of PIRADS v2 to TZ and a recent editorial Weinreb et al. [16] provided perspective and suggestions for the future. As it was very well outlined in these articles, TZ poses a special challenge for MR. Yet these fail to address one of the important examples of common misconception about TZ and different BPH types, which is the belief that glandular BPH and cystic BPH are the same and that glandular BPH appears hyperintense on T2 and ADC and therefore can easily be differentiated from TZ cancer.

Therefore, a clear lack of understanding and uncertainty regarding the MR features of different BPH types and the utility of mpMRI for PCa diagnosis that underscores further research. This study investigates the mpMRI appearance of different types of BPH (cystic, glandular and stromal) and whether quantitative mpMRI is effective in differentiating between PCa and BPH.

Materials and methods

Study patients

The study involved retrospective analysis of prospectively acquired data. It was conducted after institutional review board approval with prior informed patient consent and was HIPAA compliant. Inclusion criteria included patients with prior biopsy proven prostate cancer that underwent preoperative MRI and subsequent radical prostatectomy. Prior exclusion criteria included prior receipt of radiation or hormonal replacement therapy (leading to alterations in prostatic signal on MRI) and impaired renal function (GFR < 30 ml/min). Sixty patients that fit the criterion and were imaged at our institution between March 2014 and November 2015 were recruited for this study.

MR imaging

Patients underwent preoperative mpMRI with a 3T Philips Achieva MR scanner using a 6-channel cardiac phased array coil placed around the pelvis combined with an endorectal coil (Medrad, Bayer Healthcare). A 1-mg dose of glucagon (Glucagon, Eli Lilly & Co., Indianapolis) was injected to limit peristalsis of the rectal wall. The prostate mpMRI protocol included T2-weighted, multi-echo T2-weighted, diffusion weighted and dynamic contrast enhanced images. MR imaging parameters are described in detail in Table 1.

Histology

The individuals underwent radical prostatectomy. The prostates were fixed in formalin overnight and serially sectioned transversely, approximately in the same plane as MR images. Complete cross sections of tissue were embedded in paraffin, and whole mount hematoxylin and eosin (H&E) stained slides were made. The slides were evaluated by expert pathologists (TA and AG, 15- and 5-year experience, respectively) for prostatic adenocarcinoma and BPH. PCa and BPH were marked on the histologic slides for correlation with MR images. Cancer lesion in the transition zone greater than 5 mm in diameter was included in analysis. BPH lesions greater than 10 mm in diameter were identified in the transition zone. BPH lesions adjacent to the transition zone which were plausibly displaced from the transition zone by adjacent tumor were also included. BPH lesions were categorized as either predominantly cystic, glandular or stromal BPH. Cystic BPH has nodular, predominantly cystically dilated glands with low glandular density and minimal intervening stroma. Glandular BPH has nodular,

Table 1 MR Imaging parameters

Imaging sequence	Pulse sequence	FOV (mm)	Scan Matrix size	In plane Resolution (mm)	TE (ms)	TR (ms)	Slice Thickness (mm)	Flip angle (°)
Axial T2 W	SE-TSE	160×160	400×400	0.4×0.4	115	8230	3	90
Multi-echo T2 W (T2 mapping)	SE-TSE	160×160	212×212	0.75×0. 75	30, 60, 90, 120, 150, 180, 210, 240, 270	7850	3	90
DWI[a]	SE-EPI	180×180	120×120	1.5×1. 5	80	6093	3	90
DCE-MRI[b]	T1-FFE	250×385	200×308	1.25×1.25	3.3	4.8	3.5	10

SE spin echo, *TSE* turbo spin echo, *EPI* echo planar imaging, *FFE* fast field echo

[a]*b*-values used 0, 50, 150, 990, 1500 s/mm^2

[b]Contrast agent: gadobenate dimeglumine (MultiHance, Bracco, Minneapolis, USA) was injection at a rate of 2.0 mL/s followed by a 20-mL saline flush. Contrast dose amount was based on patient's weight (0.1 mmol/kg). DCE-MRI T1-weigthed images were taken with temporal resolution of ~ 8.3 s at 60 dynamic scan points over 8.2 min

glandular-predominant composition with gland-to-stroma ratio of 51-100%. Stromal BPH has nodular, stroma-predominant composition with gland-to-stroma ratio of 0–50%. Figure 1 shows representative images of H&E stained histology of transition zone prostate cancer and different types of BPH: cystic, glandular and stromal.

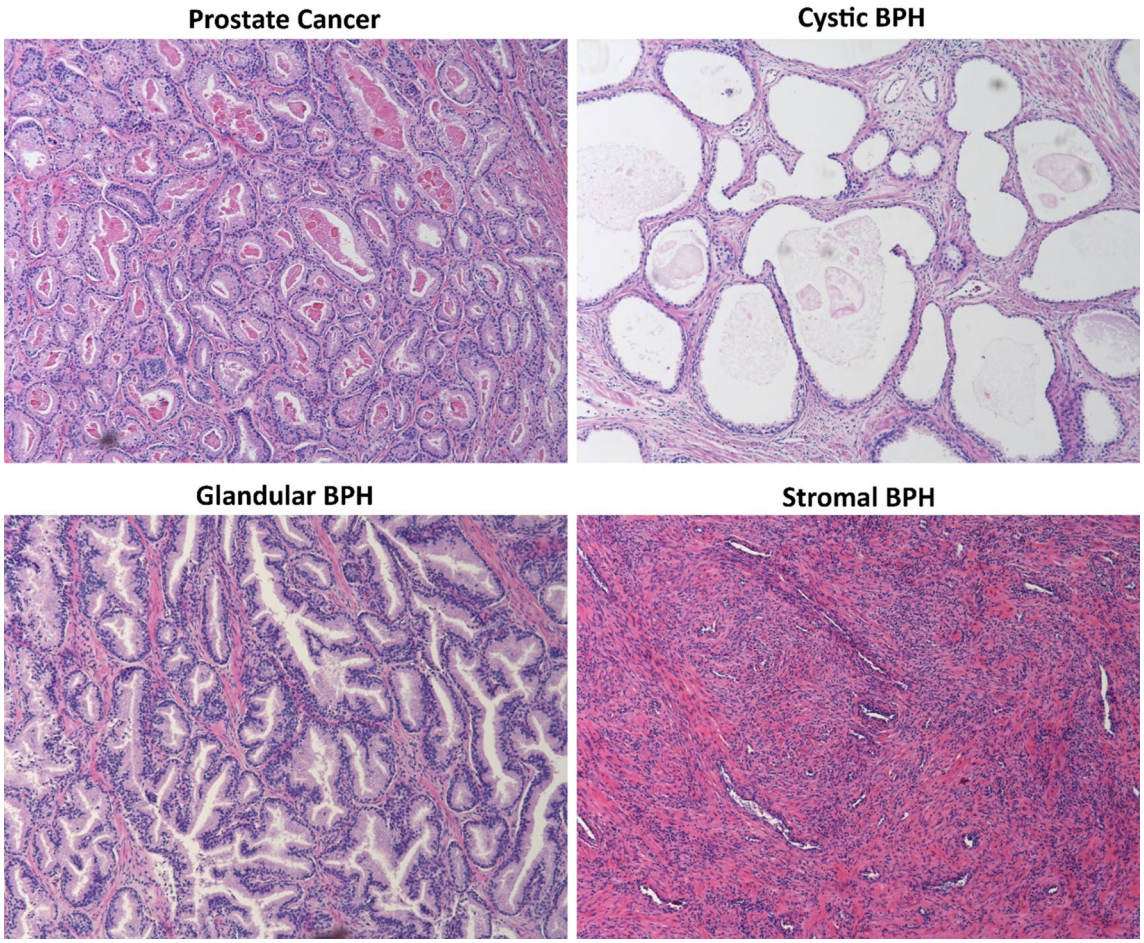

Fig. 1 Representative images of H&E stained histology (same magnification used) of transition zone prostate cancer (Gleason 3 + 4 shown) and different benign prostatic hyperplasia (BPH) types: cystic, glandular and stromal

MR image analysis

The MR image from different mpMRI sequences were co-registered to axial T2-weighted images and matched with corresponding histological sections using rigid registration in 3D Slicer (https://github.com/rcc-uchicago/PCampReview). Subsequently, MR images were analyzed by an expert radiologist (AO, 15-year experience with prostate MRI) and regions of interests (ROIs) were placed on T2-weighted images on sites of prostatectomy verified BPH and PCa in the transition zone. The ROI for the cancer lesions was drawn on the MR visible region determined by the radiologist and confirmed by registered whole mount histology. These ROIs drawn on T2 W images were the propagated to maps of all mpMRI parameters keeping the same shaped and size using 3D Slicer similar to previous studies [17, 18].

T2 values were calculated from multi-echo T2-weighted images using a mono-exponential signal decay model:

$$S = S_0 \exp(-\mathrm{TE}/\mathrm{T2})$$

where S is the signal at each echo time (TE) and S_0 is the extrapolated signal TE = 0 ms.

Apparent diffusion coefficient (ADC) was measured from diffusion weighed images using a mono-exponential signal decay:

$$S = S_0 \exp(-b \cdot \mathrm{ADC})$$

where S_0 is the maximum spin-echo signal without diffusion, S is the attenuated spin-echo signal with diffusion weighting, and b or b-value is the diffusion weighting factor.

DCE-MRI analysis was performed using the empirical mathematical model (EMM) described in Fan et al. [19] using a custom in-house program in MATLAB (Mathworks, Natick, MA) to generate quantitative DCE-MRI parameter maps. The initial time of enhancement for each voxel was found using an iterative method described in a previous study [17]. The baseline signal intensity value (S_0) of each voxel was calculated by averaging the signal intensity ($S(t)$) of the five pre-contrast time points. Subsequently, the percentage signal enhancement (PSE) as a function of time was calculated as:

$$\mathrm{PSE}(t) = \frac{S(t) - S_0}{S_0} \times 100$$

The maximum intensity projection (MIP) maps were generated by finding the maximum PSE value of each voxel. The PSE curve of standard dose data was fitted with the EMM on a voxel-by-voxel basis using a nonlinear least-squares algorithm using the following equation:

$$\mathrm{PSE}(t) = A\left(1 - e^{-\alpha t}\right)e^{-\beta t}$$

where A is the amplitude of PSE, α is the signal enhancement or uptake rate (% per second), and β is the washout rate (% per second).

Statistical analysis

Statistical analysis was performed using SPSS (IBM Corporation, Armonk, NY). The difference between means of measured mpMRI parameters was assessed by a one-way ANOVA with post hoc Tukey's HSD test. Significance level was corrected using Bonferroni correction for three post hoc comparisons, and the significance value was set as $p < 0.01$ ($0.05/3 = 0.017 \sim 0.01$). Receiver operating characteristic (ROC) analysis was used to evaluate the performance of the various mpMRI parameters in differentiating PCa from BPH. The area under the ROC curve (AUC) was reported. The optimal cutoff value was reported for effective quantitative mpMRI parameters in differentiating PCa from BPH based on the Youden's index.

Results

The mean age of patients was 58 years (range 40-72 years), and mean PSA level was 8.33 ng/mL (range 1.76–66.05 ng/mL) prior to MR imaging. A total of 106 BPH nodules were identified in the 60 patients included in this study. They were categorized as either predominantly cystic BPH ($n = 25$), glandular BPH ($n = 60$) or stromal BPH ($n = 21$). Glandular BPH was the most common BPH types (60 of 106 = 57%). BPH nodules (> 10 mm) were not identified in only three patients. In addition, a total of 34 prostate cancer lesions were identified in the transition zone, with 12 Gleason 3 + 3, 19 Gleason 3 + 4, 2 Gleason 4 + 3 and 1 Gleason 4 + 5.

Figures 2, 3, 4, 5 are representative images showing mpMRI appearance of transition zone PCa (Fig. 2) and different types of BPH: cystic (Fig. 3), glandular (Fig. 4) and stromal (Fig. 5) along with corresponding histology section (H&E). Table 2 and Fig. 6 show quantitative mpMRI results from prostate cancer and different types of BPH. The results from ROC analysis showing AUC values representing the diagnostic accuracy in differentiating prostate cancer from BPH are shown in Table 3.

ADC values

The mean ADC values were significantly lower ($F = 51.04$, $p < 0.001$) in PCa (0.99 ± 0.27 μm^2/ms) compared to all types of BPH (cystic 1.92 ± 0.43, glandular 1.31 ± 0.22, stromal 1.35 ± 0.41 μm^2/ms (post hoc analysis shows *$p < 0.001$ for differentiation of PCa from each BPH type*). In addition, ADC values for cystic BPH there were significantly higher than glandular ($p < 0.001$) and stromal ($p < 0.001$) BPH. However, no significant difference ($p = 0.72$) in ADC values between glandular and stromal BPH was found. ROC analysis showed that ADC is highly effective in differentiating PCa from BPH evidenced by high significant AUC

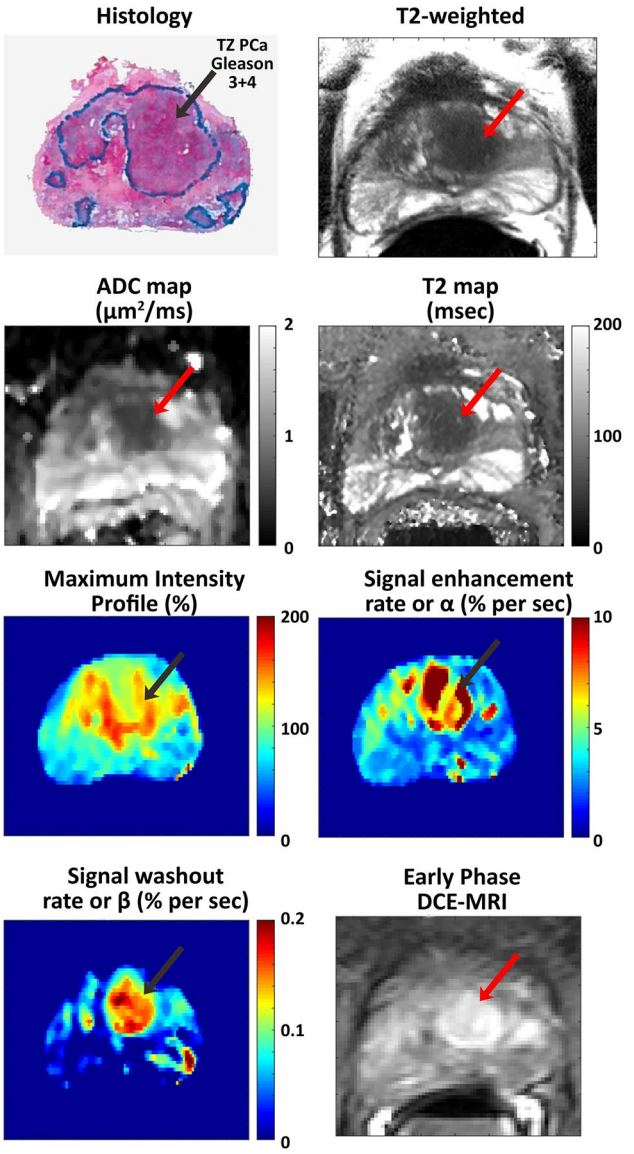

Fig. 2 67 years old patient with PSA level of 9.45 ng/mL with transition zone prostate cancer (Gleason 3+4). Representative images showing mpMRI appearance of transition zone prostate cancer (ADC = 0.58 ± 0.09 μm²/ms, T2 = 60.6 ± 8.1 ms, MIP = 119.6%, α = 10.37% per second, β = 0.152% per second) along with corresponding histological section

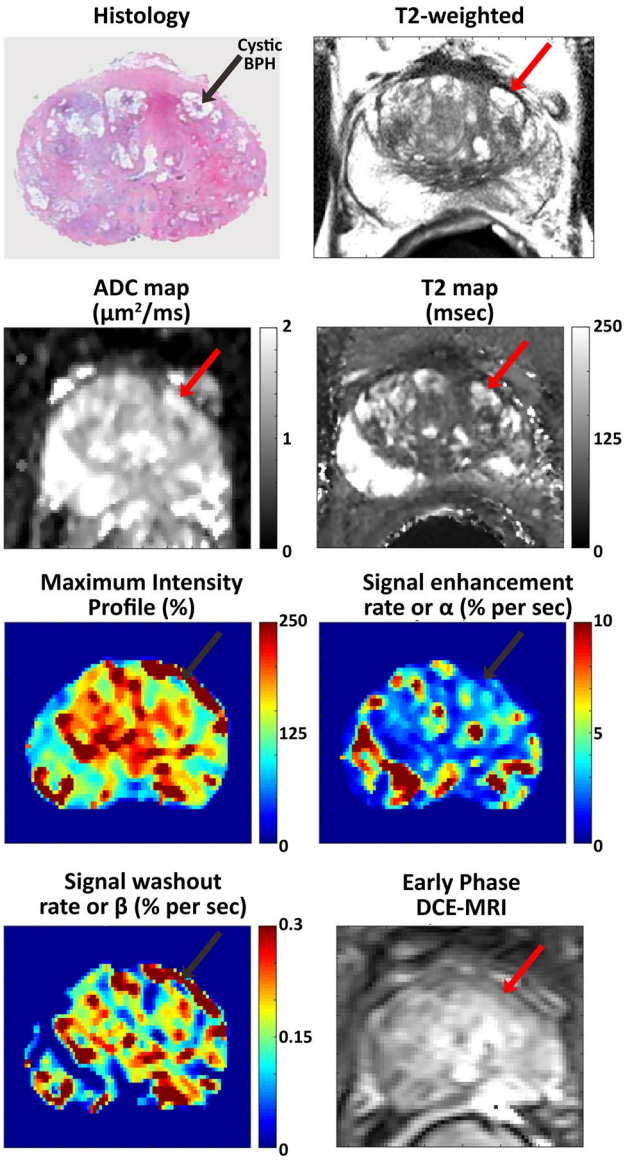

Fig. 3 56 years old patient with PSA level of 5.33 ng/mL with cystic BPH. Representative images showing mpMRI appearance of cystic BPH (ADC = 1.66 ± 0.19 μm²/ms, T2 = 182.6 ± 59.2 ms, MIP = 131.1%, α = 2.56% per second, β = 0.165% per second) along with corresponding histological section

values (0.82–0.99 for different BPH types, 0.87 overall). The optimal cutoff value for ADC to differentiate PCa from all BPH types based on the Youden's index is 1.16 μm²/ms (83.8% sensitivity and 76.5% specificity on the ROC curve). The optimal cutoff value for ADC to differentiate PCa from cystic BPH based on the Youden's index is 1.29 μm²/ms (100.0% sensitivity and 85.3% specificity on the ROC curve). The optimal cutoff value for ADC to differentiate PCa from glandular BPH based on the Youden's index is 1.15 μm²/ms (78.0% sensitivity and 76.5% specificity on the ROC curve). The optimal cutoff value for ADC to differentiate PCa from stromal BPH based on the Youden's index is 1.36 μm²/ms (71.4% sensitivity and 91.2% specificity on the ROC curve).

Quantitative T2 values

Quantitative T2 values ($F = 38.16$, $p < 0.001$) were significantly different in these different groups. However, post hoc test showed significantly lower ($p < 0.001$) T2 values in PCa (93.1 ± 24.1 ms) than in cystic BPH (242.8 ± 117.9 ms) only, while glandular ($p = 0.27$) and

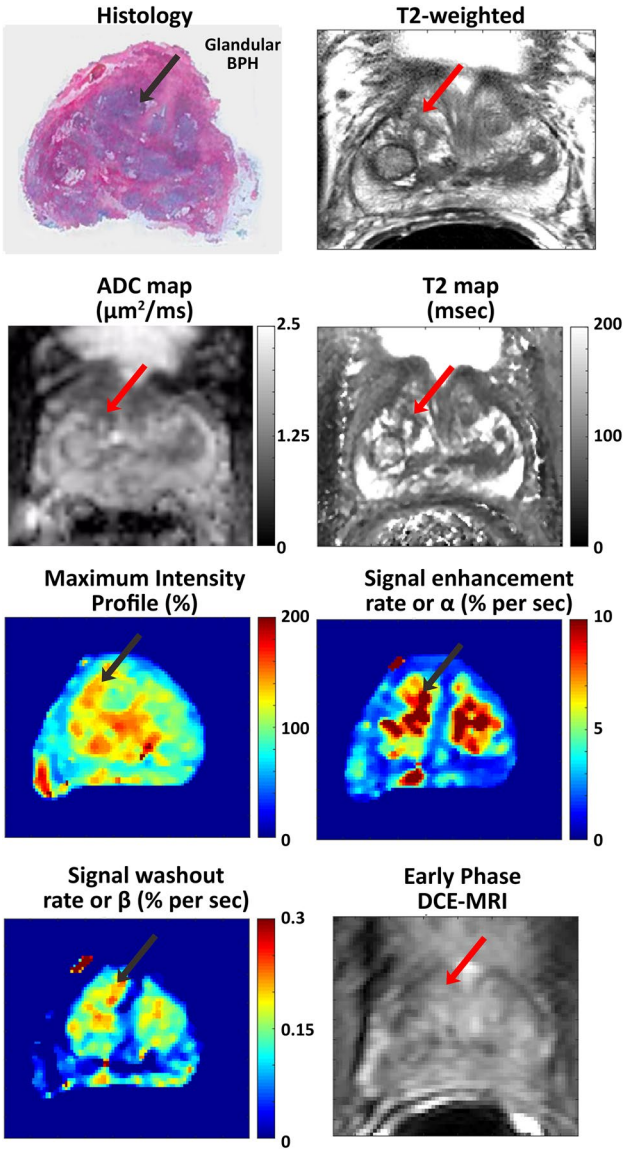

Fig. 4 68 years old patient with PSA level of 4.88 ng/mL with glandular BPH. Representative images showing mpMRI appearance of glandular BPH (ADC = 1.29 ± 0.39 μm²/ms, T2 = 123.1 ± 48.2 ms, MIP = 125.3%, α = 7.30% per second, β = 0.128% per second) along with corresponding histological section

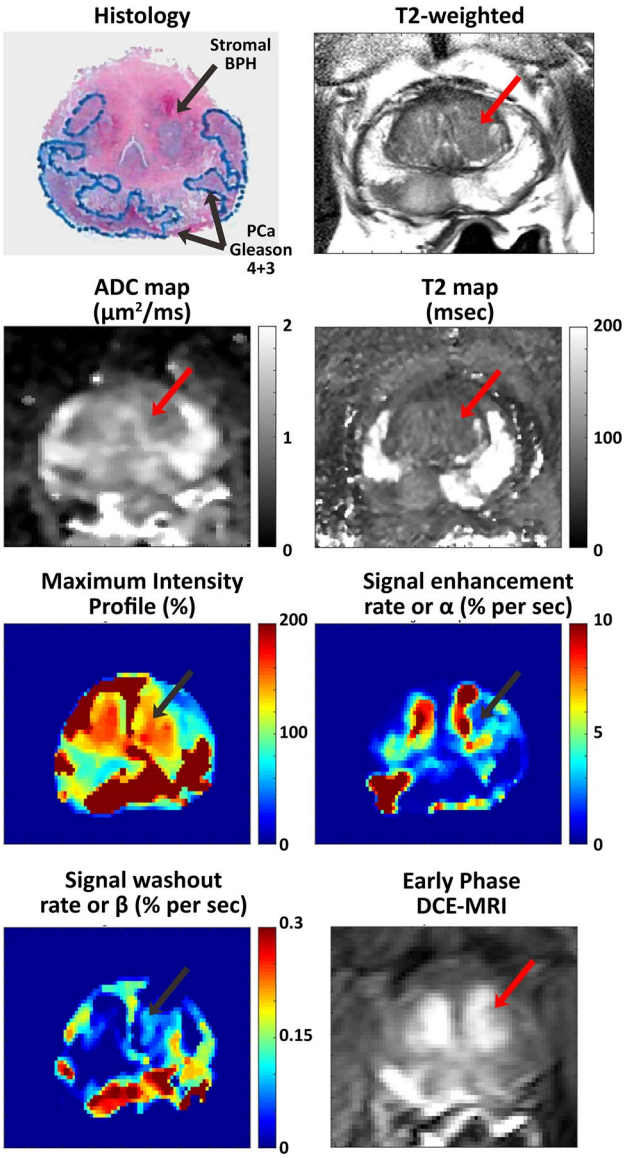

Fig. 5 59 years old patient with PSA level of 13.25 ng/mL with stromal BPH. Representative images showing mpMRI appearance of stromal BPH (ADC = 1.00 ± 0.12 μm²/ms, T2 = 92.5 ± 7.8 ms, MIP = 157.8%, α = 7.08% per second, β = 0.025% per second) along with corresponding histological section

stromal BPH ($p = 0.99$) showed no significant difference from PCa. Additionally, cystic BPH had significantly higher T2 values than both glandular ($p < 0.001$) and stromal BPH ($p < 0.001$), while there was no significant difference ($p = 0.458$) in T2 value between glandular (115.7 ± 37.3 ms) and stromal BPH (93.9 ± 14.8 ms). ROC analysis showed that T2 values are highly effective in differentiating PCa from cystic BPH (AUC = 0.98) and only moderately effective in differentiating PCa from glandular BPH (AUC = 0.74), while stromal BPH is undistinguishable from PCa using quantitative T2 values. The optimal cutoff value for quantitative T2 value to differentiate PCa from all BPH types based on the Youden's index is 101.3 ms (64.3% sensitivity and 77.4% specificity on the ROC curve). The optimal cutoff value for quantitative T2 value to differentiate PCa from cystic BPH based on the Youden's index is 137.9 ms (95.5% sensitivity and 96.8% specificity on the ROC curve). The optimal cutoff value for quantitative T2 value to differentiate PCa from glandular BPH based on the Youden's index is 101.5 ms (61.4% sensitivity and 77.4% specificity on the ROC curve). The optimal cutoff value for quantitative T2 value to differentiate

Table 2 Quantitative mpMRI results from prostate cancer and different types of BPH

	ADC (μm^2/ms)	T2 (ms)	MIP (%)	α (% per second)	β (% per second)	Number of ROIs
Mean ± standard deviation						
Prostate cancer	0.99 ± 0.27	93.1 ± 24.1	118.7 ± 49.7	6.09 ± 3.98	0.076 ± 0.105	34
BPH (Overall)	1.47 ± 0.38	140.0 ± 83.7	125.0 ± 48.9	6.34 ± 5.95	0.065 ± 0.062	106
Cystic BPH	1.92 ± 0.43	242.8 ± 117.9	91.5 ± 38.5	4.51 ± 2.07	0.031 ± 0.088	25
Glandular BPH	1.31 ± 0.22	115.7 ± 37.3	135.5 ± 50.2	7.30 ± 7.23	0.079 ± 0.052	60
Stromal BPH	1.35 ± 0.41	93.9 ± 14.8	104.8 ± 23.8	5.18 ± 1.87	0.052 ± 0.043	21

ADC apparent diffusion coefficient, α alpha or signal enhancement rate, β beta or signal washout rate, *BPH* benign prostatic hyperplasia, *MIP* maximum intensity projection

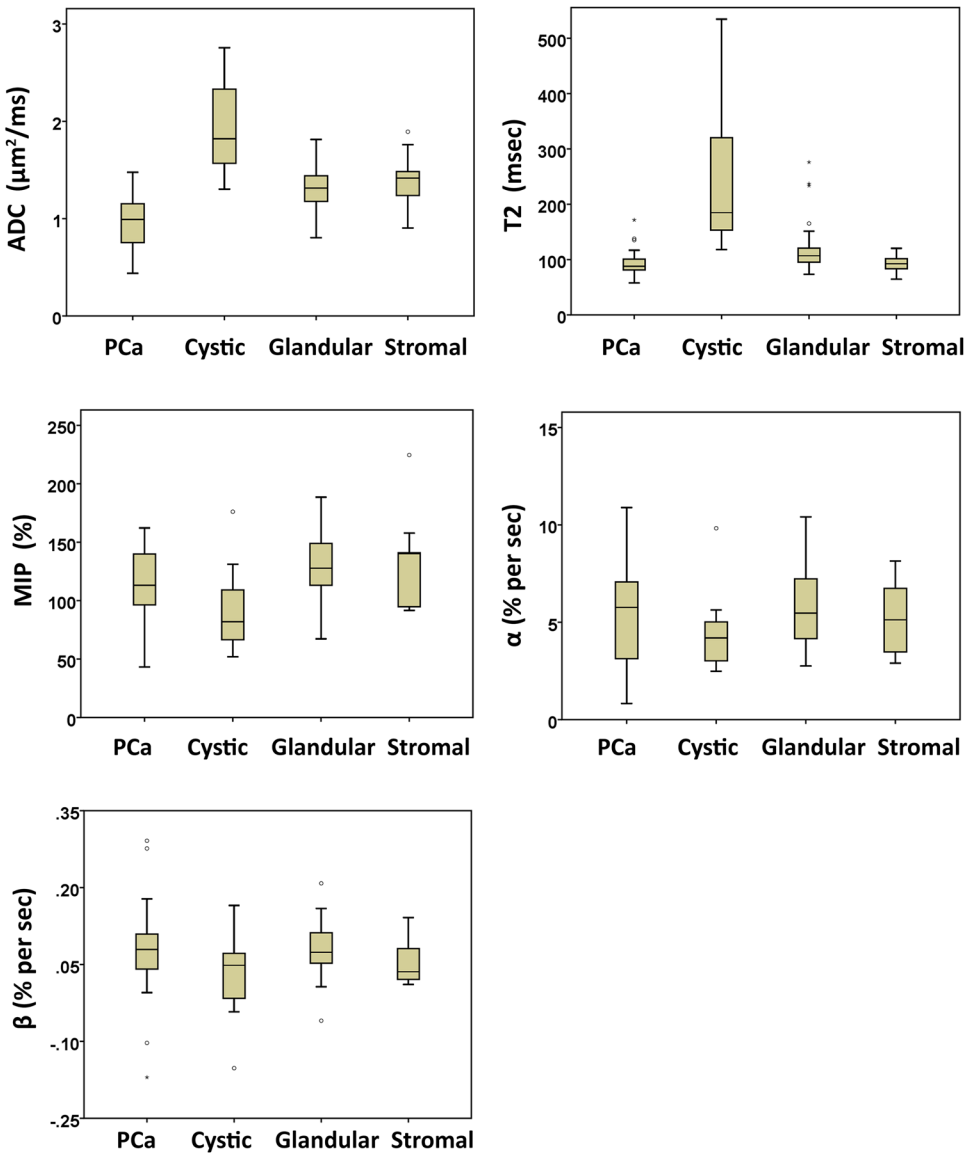

Fig. 6 Box plot of quantitative mpMRI parameters for prostate cancer (PCa) and different types of benign prostatic hyperplasia (cystic, glandular, and stromal BPH) * and ° represent outliers)

Table 3 Summary of receiver operating characteristics (roc) analysis: area under the ROC curve (AUC) for mpMRI metrics in differentiating different type of BPH from prostate cancer

	ADC (μm²/ms)	T2 (ms)	DCE-MRI		
			MIP (%)	α (% per second)	β (% per second)
AUC reported with 95% confidence interval in brackets					
BPH (Overall)	**0.87 (0.80, 0.93)** ***p < 0.001***	**0.76 (0.67, 0.86)** ***p < 0.001***	0.44 (0.29, 0.58) $p=0.07$	0.51 (0.35, 0.67) $p=0.08$	0.54 (0.38, 0.70) $p=0.60$
Cystic BPH	**0.98 (0.95, 1.00)** ***p < 0.001***	**0.98 (0.96, 1.00)** ***p < 0.001***	0.69 (0.49, 0.90) $p=0.08$	0.65 (0.45, 0.84) $p=0.18$	0.63 (0.43, 0.84) $p=0.23$
Glandular BPH	**0.82 (0.73, 0.91)** ***p < 0.001***	**0.74 (0.63, 0.86)** ***p < 0.001***	0.37 (0.21, 0.52) $p=0.10$	0.46 (0.30, 0.63) $p=0.64$	0.48 (0.31, 0.65) $p=0.81$
Stromal BPH	**0.87 (0.78, 0.97)** ***p < 0.001***	0.57 (0.40, 0.73) $p=0.44$	0.39 (0.12, 0.33) $p=0.33$	0.52 (0.31, 0.73) $p=0.87$	0.64 (0.43, 0.84) $p=0.25$

Quantitative mpMRI metrics that were significantly different from prostate cancer on ANOVA analysis with post hoc Tukey HSD are shown in bold

PCa from stromal BPH based on the Youden's index is 82.1 ms (84.2% sensitivity and 35.5% specificity on the ROC curve).

Quantitative DCE-MRI values

There is no significant difference between PCa and different BPH types for the measured quantitative DCE-MRI parameters: MIP ($F=2.59$, $p=0.06$), α ($F=0.91$, $p=0.44$) and β ($F=1.37$, $p=0.26$). ROC analysis showed the AUC values were not significant and therefore neither of the DCE-MRI parameters are effective in differentiating between PCa and BPH. In addition, DCE-MRI parameters were higher for BPH than PCa in a few cases (e.g., MIP and α were nominally higher in glandular BPH than PCa) and therefore AUC values are lower than the null hypothesis (AUC = 0.5). While there are no significant differences in DCE-MRI parameters, the results here show that increased glandular structure (cystic and stromal < glandular and PCa) leads to nominally increased quantitative DCE-MRI metrics: signal enhancement and washout rates.

Discussion

The results from this study highlight the highly heterogeneous nature of the transition zone evidenced by the different histology and quantitative mpMRI parameters seen in different BPH types. In previous studies, addressing mpMRI findings of transition zone, cystic BPH was considered a form of glandular BPH and subsequent study concluded that glandular BPH can be easily distinguished from PCa using T2 W and ADC [8]. In fact, cystic and glandular BPH are histologically distinct and these two BPH types have completely different mpMRI appearance. In addition, glandular BPH have similar T2 and DW-MRI characteristics to stromal BPH and PCa, and therefore differentiating glandular BPH and PCa is more difficult than previously considered. It critical for radiologists to be aware of the distinction between different BPH types and their appearance on mpMRI during radiopathologic correlation or performing PCa diagnosis, especially since glandular BPH was found to be the most common BPH type. This is an important update to our previous knowledge about mpMRI characteristics of the transition zone and the differentiation of PCa from BPH. Our results show that cystic BPH are characterized by high ADC and T2 values, and glandular BPH have moderately higher ADC and T2 than PCa. Stromal BPH have moderately higher ADC but similar T2 values to PCa.

Quantitative ADC values derived from diffusion weighted imaging remains the most effective parameter in differentiating BPH from PCa. These results are similar to a few previous studies [8, 12, 20–23]. Qualitative T2 values are effective in the distinction of PCa from cystic and glandular BPH; however, differentiating stromal BPH and PCa is problematic. The PI-RADS v2 consensus guidelines [24] underplays the role of DWI or ADC for scoring TZ PCa lesions. Our results show that quantitative ADC values can be used for differentiating PCa and BPH. Morphological features such as homogenous low T2 signal with ill-defined margins and lack of capsule on T2 W are recommended by PI-RADS v2 to be used for detecting PCa as demonstrated in previous studies [25, 26]. However, this study did not look at the qualitative morphological features in BPH and PCa.

BPH have similar DCE-MRI parameters and therefore mimic PCa on DCE-MRI. While some previous have noted that DCE-MRI can help in improving differentiating PCa from BPH [8, 27], other studies have shown that similar results to our study where DCE-MRI was shown to add no additional benefit for PCa detection in the transition zone [17, 28, 29]. Angiogenesis or increased micro-vessel density is generally

regarded as the reason for increased contrast uptake in cancer tissue [30, 31]. However, there is no literature to our knowledge that has investigated the difference in contrast kinetics in different tissue components. However, the results here show that increased quantitative DCE-MRI metrics: signal enhancement and washout rate are potentially related to increased glandular structure (cystic and stromal < glandular and PCa).

Prostate tissue microstructure and composition affects its appearance on MRI. Tissue components: stroma, epithelium and lumen each have distinct MR properties [32] and their composition changes with the presence of PCa [33, 34] and other benign conditions such as BPH [35, 36]. Cystic BPH is composed predominantly of expanded luminal spaces filled with luminal fluid with a minority of glandular epithelium and stroma and therefore should have high T2 and ADC values. Stromal BPH is composed primarily of fibrous and fibromuscular tissue with a minority of glandular epithelium and lumens and therefore should have intermediate ADC and low T2. Glandular BPH is composed predominantly of glandular epithelium with associated lumens and a minority of stroma and therefore should have intermediate ADC and T2 values. The results from this study follow the expected trends as discussed above.

The quantitative mpMRI parameters: ADC and T2 values used in this study which are generally used clinically for PCa detection are derived from phenomenological models. However, they provide little information regarding the underlying complex microstructure [37]. While ADC is shown to be highly effective in differentiating PCa from BPH, we speculate that recently developed structural models such as VERDICT [38], Luminal Volume Imaging [39] and Hybrid Multidimensional MRI [40] will be able to better depict heterogeneity in the transition zone and improve the differentiation of PCa from BPH due to their ability to estimate tissue composition noninvasively that have previously been shown to change with the presence and increasing Gleason grade of prostate cancer [33, 34].

Our study had a few limitations. T2-weighted imaging is the dominant sequence for PCa detection in the transition zone [24]. While we evaluated quantitative T2 values in PCa and BPH, we, however, did not evaluate visual analysis of T2-weighted images by a radiologist. Our study used EMM, a pure mathematical model instead of the more commonly used Tofts' pharmacokinetic model [41] as there are concerns regarding reliable arterial input function estimation and the assumptions made in this model may not be valid for all tissue type [42, 43] and the quantitative T1 values required for calculation of contrast media concentration may result in propagation of error and may limit diagnostic accuracy. In contrast, the EMM is easy to implement and more consistent with visual assessment of DCE-MR images and previous work has demonstrated that EMM parameters are potentially as effective as Tofts model in cancer detection [44, 45]. Nonetheless, our results highlight the difficulty in diagnosing PCa in the transition zone noted in numerous studies. As the means for quantitative mpMRI parameters are reported for each category with different populations, adjusted analysis using a larger population may be warranted for future studies. While the use of radical prostatectomy specimen is great from the perspective of having the ultimate gold standard, inclusion exclusively of men who underwent surgery biases the patient population toward a subgroup with intermediate and high-risk prostate cancer and possibly higher incidence of BPH, therefore unlikely to be representative of the general population.

In conclusion, our study showed that in contrast to current knowledge, cystic and glandular BPH have distinct mpMRI characteristics and it is important for radiologists to be aware of this distinction while performing radiopathologic correlation and trying to understand MR features of different histopathologic components of the prostate. Glandular BPH is not hyperintense on ADC and T2 as previously thought and has similar quantitative mpMRI measurements to stromal BPH. Our study confirmed that mpMRI and specifically quantitative ADC values can be used for differentiating PCa and BPH, improving PCa diagnosis in the transition zone. However, DCE-MRI metrics are not effective in distinguishing PCa and BPH. These results highlight the difficulty in differentiating between prostate cancer and BPH due to the heterogeneous nature prostatic tissue in the transition zone. Quantitative ADC values derived from diffusion weighted imaging are the most effective parameter in differentiating BPH from PCa.

Disclosures Dr Aytekin Oto has the following disclosures - Research Grant, Koninklijke Philips NV Research Grant, Guerbet SA Research Grant, Profound Medical Inc. Medical Advisory Board, Profound Medical Inc Speaker, Bracco Group.

Funding Philips Healthcare and National Institutes of Health (NIH R01 CA172801 and NIH 1S10OD018448-01).

Compliance with ethical standards

Conflict of interest The authors declare that they have no conflict of interests.

Ethical approval The study was conducted after institutional review board approval and was compliant with Health Insurance Portability and Accountability Act.

Informed consent Informed patient consent was obtained for recruiting patients in this study.

References

1. Siegel RL, Miller KD, Jemal A. Cancer statistics, 2018. CA: A Cancer Journal for Clinicians. 2018; 68(1):7-30.

2. McNeal JE, Redwine EA, Freiha FS, Stamey TA. Zonal distribution of prostatic adenocarcinoma. Correlation with histologic pattern and direction of spread. The American journal of surgical pathology. 1988; 12(12):897-906.
3. McNeal J, Noldus J. Limitations of transition zone needle biopsy findings in the prediction of transition zone cancer and tissue composition of benign nodular hyperplasia. Urology. 1996; 48(5):751-6.
4. Koppie TM, Bianco FJ, Kuroiwa K, et al. The clinical features of anterior prostate cancers. BJU international. 2006; 98(6):1167-71.
5. Berry SJ, Coffey DS, Walsh PC, Ewing LL. The development of human benign prostatic hyperplasia with age. J Urol. 1984; 132(3):474-9.
6. Schiebler ML, Tomaszewski JE, Bezzi M, et al. Prostatic carcinoma and benign prostatic hyperplasia: correlation of high-resolution MR and histopathologic findings. Radiology. 1989; 172(1):131-7.
7. Turnbull LW, Buckley DL, Turnbull LS, Liney GP, Knowles AJ. Differentiation of prostatic carcinoma and benign prostatic hyperplasia: Correlation between dynamic Gd-DTPA-enhanced MR imaging and histopathology. Journal of Magnetic Resonance Imaging. 1999; 9(2):311-6.
8. Oto A, Kayhan A, Jiang Y, et al. Prostate Cancer: Differentiation of Central Gland Cancer from Benign Prostatic Hyperplasia by Using Diffusion-weighted and Dynamic Contrast-enhanced MR Imaging. Radiology. 2010; 257(3):715-23.
9. Kitzing YX, Prando A, Varol C, Karczmar GS, Maclean F, Oto A. Benign Conditions That Mimic Prostate Carcinoma: MR Imaging Features with Histopathologic Correlation. RadioGraphics. 2016; 36(1):162-75.
10. Epstein JI, Paull G, Eggleston JC, Walsh PC. Prognosis of Untreated Stage A1 Prostatic Carcinoma: A Study of 94 Cases with Extended Followup. The Journal of urology. 1986; 136(4):837-9.
11. Blute ML, Zincke H, Farrow GM. Long-Term Followup of Young Patients with Stage a Adenocarcinoma of the Prostate. The Journal of urology. 1986; 136(4):840-3.
12. Kim CK, Park BK, Lee HM, Kwon GY. Value of diffusion-weighted imaging for the prediction of prostate cancer location at 3T using a phased-array coil: preliminary results. Invest Radiol. 2007; 42(12):842-7.
13. Tamada T, Sone T, Jo Y, et al. Apparent diffusion coefficient values in peripheral and transition zones of the prostate: Comparison between normal and malignant prostatic tissues and correlation with histologic grade. J Magn Reson Imaging. 2008; 28(3):720-6.
14. Ishida J, Sugimura K, Okizuka H, et al. Benign prostatic hyperplasia: value of MR imaging for determining histologic type. Radiology. 1994; 190(2):329-31.
15. Thai JN, Narayanan HA, George AK, et al. Validation of PI-RADS Version 2 in Transition Zone Lesions for the Detection of Prostate Cancer. Radiology. 2018; 288(2):485-91.
16. Weinreb JC. Organized Chaos: Does PI-RADS Version 2 Work in the Transition Zone? Radiology. 2018; 288(2):492-4.
17. Chatterjee A, He D, Fan X, et al. Performance of ultrafast DCE-MRI for diagnosis of prostate cancer. Academic Radiology. 2018; 25(3):349-58.
18. He D, Chatterjee A, Fan X, et al. Feasibility of Dynamic Contrast-Enhanced Magnetic Resonance Imaging Using Low-Dose Gadolinium: Comparative Performance With Standard Dose in Prostate Cancer Diagnosis. Investigative Radiology. 2018; 53(10):609-15.
19. Fan X, Medved M, River JN, et al. New model for analysis of dynamic contrast-enhanced MRI data distinguishes metastatic from nonmetastatic transplanted rodent prostate tumors. Magnetic resonance in medicine. 2004; 51(3):487-94.
20. Akin O, Sala E, Moskowitz CS, et al. Transition Zone Prostate Cancers: Features, Detection, Localization, and Staging at Endorectal MR Imaging. Radiology. 2006; 239(3):784-92.
21. Kayhan A, Fan X, Oommen J, Oto A. Multi-parametric MR imaging of transition zone prostate cancer: Imaging features, detection and staging. World Journal of Radiology. 2010; 2(5):180-7.
22. Sato C, Naganawa S, Nakamura T, et al. Differentiation of noncancerous tissue and cancer lesions by apparent diffusion coefficient values in transition and peripheral zones of the prostate. Journal of Magnetic Resonance Imaging. 2005; 21(3):258-62.
23. Noworolski SM, Vigneron DB, Chen AP, Kurhanewicz J. Combined Dynamic Contrast-Enhanced MRI and MR Diffusion Imaging to Distinguish Between Glandular and Stromal Prostatic Tissues. Magnetic Resonance Imaging. 2008; 26(8):1071-80.
24. Weinreb JC, Barentsz JO, Choyke PL, et al. PI-RADS Prostate Imaging – Reporting and Data System: 2015, Version 2. European Urology. 2016; 69(1):16-40.
25. Li H, Sugimura K, Kaji Y, et al. Conventional MRI Capabilities in the Diagnosis of Prostate Cancer in the Transition Zone. American Journal of Roentgenology. 2006; 186(3):729-42.
26. Guneyli S, Ward E, Thomas S, et al. Magnetic resonance imaging of benign prostatic hyperplasia. Diagnostic and Interventional Radiology. 2016; 22(3):215-9.
27. Kozlowski P, Chang SD, Jones EC, Berean KW, Chen H, Goldenberg SL. Combined diffusion-weighted and dynamic contrast-enhanced MRI for prostate cancer diagnosis—Correlation with biopsy and histopathology. Journal of Magnetic Resonance Imaging. 2006; 24(1):108-13.
28. Rosenkrantz AB, Kim S, Campbell N, Gaing B, Deng F-M, Taneja SS. Transition Zone Prostate Cancer: Revisiting the Role of Multiparametric MRI at 3 T. American Journal of Roentgenology. 2015; 204(3):W266-W72.
29. Chesnais AL, Niaf E, Bratan F, et al. Differentiation of transitional zone prostate cancer from benign hyperplasia nodules: Evaluation of discriminant criteria at multiparametric MRI. Clinical Radiology. 2013; 68(6):e323-e30.
30. Schlemmer H-P, Merkle J, Grobholz R, et al. Can pre-operative contrast-enhanced dynamic MR imaging for prostate cancer predict microvessel density in prostatectomy specimens? European Radiology. 2004; 14(2):309-17.
31. Verma S, Turkbey B, Muradyan N, et al. Overview of dynamic contrast-enhanced MRI in prostate cancer diagnosis and management. AJR Am J Roentgenol. 2012; 198(6):1277-88.
32. Bourne RM, Kurniawan N, Cowin G, et al. Microscopic diffusivity compartmentation in formalin-fixed prostate tissue. Magn Reson Med. 2012; 68(2):614-20.
33. Chatterjee A, Watson G, Myint E, Sved P, McEntee M, Bourne R. Changes in Epithelium, Stroma, and Lumen Space Correlate More Strongly with Gleason Pattern and Are Stronger Predictors of Prostate ADC Changes than Cellularity Metrics. Radiology. 2015; 277(3):751-62.
34. Langer DL, van der Kwast TH, Evans AJ, et al. Prostate tissue composition and MR measurements: investigating the relationships between ADC, T2, K(trans), v(e), and corresponding histologic features. Radiology. 2010; 255(2):485-94.
35. Bartsch G, Muller HR, Oberholzer M, Rohr HP. Light microscopic stereological analysis of the normal human prostate and of benign prostatic hyperplasia. J Urol. 1979; 122(4):487-91.
36. Siegel YI, Zaidel L, Hammel I, Korczak D, Lindner A. Morphometric evaluation of benign prostatic hyperplasia. Eur Urol. 1990; 18(1):71-3.
37. Bourne R, Panagiotaki E. Limitations and Prospects for Diffusion-Weighted MRI of the Prostate. Diagnostics. 2016; 6(2):21.
38. Panagiotaki E, Chan RW, Dikaios N, et al. Microstructural Characterization of Normal and Malignant Human Prostate Tissue

With Vascular, Extracellular, and Restricted Diffusion for Cytometry in Tumours Magnetic Resonance Imaging. Investigative Radiology. 2015; 50(4):218-27.
39. Sabouri S, Chang SD, Savdie R, et al. Luminal Water Imaging: A New MR Imaging T2 Mapping Technique for Prostate Cancer Diagnosis. Radiology. 2017; 284(2):451-9.
40. Chatterjee A, Bourne R, Wang S, et al. Diagnosis of Prostate Cancer with Noninvasive Estimation of Prostate Tissue Composition by Using Hybrid Multidimensional MR Imaging: A Feasibility Study. Radiology. 2018; 287(3):864-72.
41. Tofts PS, Brix G, Buckley DL, et al. Estimating kinetic parameters from dynamic contrast-enhanced t1-weighted MRI of a diffusable tracer: Standardized quantities and symbols. Journal of Magnetic Resonance Imaging. 1999; 10(3):223-32.
42. Buckley DL. Uncertainty in the analysis of tracer kinetics using dynamic contrast-enhanced T1-weighted MRI. Magnetic Resonance in Medicine. 2002; 47(3):601-6.
43. Isebaert S, De Keyzer F, Haustermans K, et al. Evaluation of semi-quantitative dynamic contrast-enhanced MRI parameters for prostate cancer in correlation to whole-mount histopathology. European Journal of Radiology. 2012; 81(3):e217-e22.
44. Jansen SA, Fan X, Medved M, et al. Characterizing early contrast uptake of ductal carcinoma in situ with high temporal resolution dynamic contrast-enhanced MRI of the breast: a pilot study. Phys Med Biol. 2010; 55(19):473–85.
45. Fan X, Medved M, Karczmar GS, et al. Diagnosis of suspicious breast lesions using an empirical mathematical model for dynamic contrast-enhanced MRI. Magnetic Resonance Imaging. 2007; 25(5):593-603.

Publisher's Note Springer Nature remains neutral with regard to jurisdictional claims in published maps and institutional affiliations.